

Phase separation and the segregation principle in the infinite- U spinless Falicov-Kimball model

J. K. Freericks[†], Ch. Gruber^{*}, and N. Macris^{*}

[†]*Department of Physics, Georgetown University, Washington, DC 20057 USA*

^{*}*Institut de Physique Théorique, Ecole Polytechnique Fédérale de Lausanne, PHB-Ecublens, CH-1015, Lausanne, Switzerland*

Abstract

The simplest statistical-mechanical model of crystalline formation (or alloy formation) that includes electronic degrees of freedom is solved exactly in the limit of large spatial dimensions and infinite interaction strength. The solutions contain both second-order phase transitions and first-order phase transitions (that involve phase-separation or segregation) which are likely to illustrate the basic physics behind the static charge-stripe ordering in cuprate systems. In addition, we find the spinodal-decomposition temperature satisfies an approximate scaling law.

Principle PACS number 71.20.Cf. Secondary PACS numbers 71.30.+h and 71.28.+d

I. INTRODUCTION

The most fundamental problem in solid-state physics is to understand why elements (and most compounds) crystallize in ordered periodic structures, for this forms the basis of all of solid-state physics. While it is well known that the driving principle behind this ordering is a lowering of the ground-state energy of the material, and there has been significant progress with *ab initio* methods to predict the ground-state properties of these ordered phases in real materials, there still are no exactly solvable models for crystal formation that describe the statistical-mechanical mechanism behind the ordering of the electrons and ions on a periodic lattice. Furthermore, it is not understood what the physical mechanisms are that are necessary for creating a crystallized state. This crystallization problem is ubiquitous; it also describes the statistical mechanics behind binary-alloy formation or phase separation since the two problems can be mapped onto each other (as described below), and it may also describe the physics behind charge-stripe formation in the cuprates.

It may sound surprising that no solvable statistical-mechanical model for crystallization exists, since a statistical-mechanical model for magnetic order has been known ever since Onsager solved the two-dimensional Ising model¹. Onsager's solution produced a paradigm for understanding phase transitions in many different physical systems and provided a textbook example of much of the theory behind modern critical phenomena. In fact, Lee and Yang² modified the Ising model to consider the magnetic order in an external magnetic field, and mapped the problem onto a lattice gas, where the up spins denoted sites occupied by ions, and the down spins denoted empty sites. Onsager's method of solution does not extend to the case of a finite magnetic field, so no exact results are known for the lattice gas, except in the case where the number of ions equals one half the number of lattice sites, which corresponds to the zero-field case. These models of crystallization neglect the electronic degrees of freedom of the valence electrons, and hence are not directly applicable to real materials such as metals and alloys.

It turns out that the Ising model, and many other models for magnetism, simplify when they are examined in high dimensions. In fact, the Ising model is solved by a static mean field theory in four and higher dimensions. A similar situation is expected for electronic problems, except they remain nontrivial even in the infinite-dimensional limit^{3,4}. Metzner and Vollhardt showed that the electronic problem requires a dynamical mean-field theory for its solution in infinite dimensions. Furthermore, a wide range of evidence indicates that this dynamical mean-field theory provides a quantitative approximation to the solutions of correlated electron problems in three dimensions (at least if one is not too close to a critical point). In fact, it is precisely the nonuniversal properties (such as a transition temperature) that the dynamical mean-field theory determines accurately, and its solution provides a wealth of information on the qualitative behavior of the model studied. We employ the dynamical mean-field theory here to produce an exact solution of the crystallization problem which includes the electronic degrees of freedom.

The simplest model that can describe crystallization and include electronic degrees of freedom is the spinless Falicov-Kimball model⁵ which consists of two kinds of particles: localized ions and itinerant (spinless) electrons. The localized ions ($w_i = 0$ or 1) occupy sites on a lattice in real space with an energy E , and the electrons can hop (with a hopping integral $-t^*/[2\sqrt{d}]$) between neighboring lattice sites. In addition, there is a screened Coulomb

interaction U between electrons and ions that occupy the same lattice site. Since the electrons do not interact with each other, the “spin” degree of freedom is unimportant, and is neglected. The Hamiltonian is

$$H = -\frac{t^*}{2\sqrt{d}} \sum_{\langle i,j \rangle} c_i^\dagger c_j + E \sum_i w_i + U \sum_i c_i^\dagger c_i w_i, \quad (1)$$

with c_i^\dagger (c_i) the creation (annihilation) operator for electrons at site i , and w_i denoting the ion occupancy at site i . We use $t^* = 1$ as the energy scale.

The Falicov-Kimball model can be viewed as a simplified approximation to a real material in a variety of ways. If the material has a single valence electron, and only one electronic band lies near the Fermi level, then the crystallization problem would correspond to the case where the electron and ion concentrations (ρ_e and ρ_i) are the same (which is called the neutral case), since one electron is donated by each ion. If, instead, there are many bands near the Fermi level, then one can map the combined bands into a single “effective” band which will have an electron filling determined by the average filling of the electrons in the most important band. In this case, each ion may donate only a fraction of an electron to the crystal, because the rest of the electron goes into other hybridized bands that lie close to the Fermi level. Hence, one may find it useful to also consider nonneutral cases for the crystallization problem, where the electron and ion concentrations are not equal. This model can also be mapped onto the binary alloy problem, where a site occupied by an ion is mapped to a site occupied by an A ion and a site unoccupied by an ion is mapped to a site occupied by a B ion, and the screened Coulomb interaction is mapped to the difference in the site energies for electrons on an A ion versus on a B ion.

As it stands, the Falicov-Kimball model doesn’t appear to be a many-body problem at all, since the ions are localized and do not move, which implies that the quantum-mechanical problem for the electrons can be solved by diagonalizing a single-particle problem of an electron moving in the potential determined by the given configuration of the ions $\{w_i\}$. The many-body problem aspects enter by taking an annealed average over all possible ion configurations with the chosen ion concentration. This produces long-range interactions between the ions, that can cause them to order or phase separate at low temperatures.

Much is already known about the physics of the Falicov-Kimball model (as reviewed by Gruber and Macris⁶). In the neutral case where each particle concentration equals $1/2$, Lieb and Kennedy⁷ and Brandt and Schmidt⁸ proved that the system always orders in an alternating “chessboard” phase at a finite transition temperature in all dimensions greater than 1. This ordered phase can be interpreted as the transition from a high-temperature homogeneous (liquid/gas) phase to a low-temperature ordered (solid) phase. The appearance of a low-temperature ordered phase follows as a consequence of the Pauli exclusion principle, since Lieb and Kennedy also showed that if the itinerant particles were Bosons instead of electrons, they would clump together and not form a periodically ordered ground state.

The Falicov-Kimball model is expected to be in the same universality class as the Ising model, but, because of the electronic degrees of freedom, one needs to solve the full statistical model to determine the “effective magnetic exchange parameters” between different lattice sites. The parameters can be extracted in a systematic expansion if the electronic kinetic energy (the hopping term) is taken as a perturbation,^{9–11} but such an analysis is only valid in the strong-coupling regime, and rapidly becomes problematic. *It is precisely this*

complication that has frustrated attempts at finding an exact solution to the crystallization problem when electronic degrees of freedom are introduced.

The one-dimensional limit of the Falicov-Kimball model has also been extensively studied. Here there are no finite-temperature phase transitions, but the system can have phase transitions in the ground state. The first attempt at studying the one-dimensional Falicov-Kimball model proceeded along the lines of *ab initio* band-structure calculations for real materials—a small number of candidate ion configurations were chosen for the ground state, and a restricted phase diagram was determined for all structures within the subset¹². The numerical solutions produced two conjectures: the first was a result for the case where $\rho_e \neq 1 - \rho_i$, which stated that if the screened Coulomb interaction U was large enough, then the system would segregate into an empty lattice (with no ions and all the electrons), and a full lattice (with all the ions and no electrons). The second was a generalization of the Peierls instability, which says that in the small U limit the system will order in such a fashion that the ions produce a band structure that has a maximal gap at the Fermi level. This first conjecture (the segregation principle) was later proven to be true by Lemberger¹³ while the second conjecture was shown to be false if the electron concentration was sufficiently far from half-filling. In that case, the system would phase separate between the empty lattice, and an optimally chosen ion structure that had the Fermi level lying in the gap¹⁴.

The other limit that has been extensively studied is the large-dimensional limit where Brandt and Mielsch¹⁵ provided the solution of the transition temperature as a function of U for the half-filled symmetric case. Their solution involves solving a coupled set of transcendental equations which display first and second-order phase transitions. Freericks¹⁶ later showed that the model (on a hypercubic lattice) also displayed incommensurate order and segregation.

There are two kinds of lattices that are usually investigated in the large coordination-number limit: the hypercubic lattice, which is the generalization of the cubic lattice to large dimensions; and the Bethe lattice, which is a thermodynamic limit of the Cayley tree when the number of nearest neighbors becomes large. The noninteracting band structure for the hypercubic lattice produces a density of states that is a Gaussian [$\rho_H(\epsilon) = \exp(-\epsilon^2)/\sqrt{\pi}$], while on the Bethe lattice the density of states is Wigner's semicircle [$\rho_B(\epsilon) = \sqrt{4 - \epsilon^2}/(2\pi)$]. The hypercubic density of states has an infinite bandwidth, but most of the weight lies within a range of ± 2 about the origin. The Bethe lattice density of states has the same behavior as a three-dimensional system at the band edge (square-root behavior) but has no van Hove singularities in the interior of the band. Because both density of states are nontrivial, the many-body problem maintains much of its rich behavior that arises from the competition between kinetic-energy effects and interaction-energy effects. In particular, the Falicov-Kimball model continues to have phase transitions in the large coordination number limit, but the transitions have mean-field theory exponents.

In this contribution, we examine what happens in the case when the Coulomb interaction becomes infinite $U \rightarrow \infty$ (the attractive case is equivalent to this case through a particle-hole transformation of the electrons, which carries $\rho_e \rightarrow 1 - \rho_e$). In this case, the electrons avoid the sites of the lattice occupied by the ions, so the electron concentration varies from zero up to $1 - \rho_i$. We investigated the non-unit-density cases, where the electron concentration was restricted to $0 \leq \rho_e < 1 - \rho_i$. In Section II the formalism and results for calculations on the Bethe lattice are presented. In Section III, results for the hypercubic lattice are given

and in Section IV we present our conclusions.

II. FORMALISM AND RESULTS FOR THE BETHE LATTICE

In the thermodynamic limit, the local lattice Green's function is defined to be

$$G_n = G(i\omega_n) = - \int_0^\beta d\tau e^{i\omega_n \tau} \frac{\text{Tr} \langle e^{-\beta(H-\mu N)} T_\tau c(\tau) c^\dagger(0) \rangle}{\text{Tr} \langle e^{-\beta(H-\mu N)} \rangle}, \quad (2)$$

where $i\omega_n = i\pi T(2n + 1)$ is the Fermionic Matsubara frequency, $\beta = 1/T$ is the inverse temperature, μ is the electron chemical potential, and T_τ denotes τ -ordering. The angle brackets in Eq. (2) denote the sum over ionic configurations. The local Green's function is determined by mapping onto an atomic problem in a time-dependent field, with the following action

$$S_{at} = \int_0^\beta d\tau \int_0^\beta d\tau' c^\dagger(\tau) G_0^{-1}(\tau - \tau') c(\tau') + U \int_0^\beta d\tau c^\dagger(\tau) c(\tau) w + Ew, \quad (3)$$

where $w = 0, 1$ is the ion number for the atomic site and G_0^{-1} is the mean-field or effective-medium Green's function, which is determined self-consistently (as described below). The atomic Green's function, with the action in Eq. (3), is computed to be

$$G_n = \frac{1 - \rho_i}{G_0^{-1}(i\omega_n)} + \frac{\rho_i}{G_0^{-1}(i\omega_n) - U}, \quad (4)$$

with ρ_i the average ion density $\langle w \rangle$. On the other hand, the local lattice Green's function satisfies

$$G_n = \int_{-\infty}^{\infty} d\epsilon \frac{\rho(\epsilon)}{i\omega_n + \mu - \Sigma_n - \epsilon}, \quad (5)$$

where $\rho(\epsilon)$ is the noninteracting density of states for the infinite lattice and Σ_n is the self-energy. The self-consistency relation is that the self-energy Σ_n in Eq. (5) must coincide with the self-energy of the atomic problem, i. e.

$$\Sigma(i\omega_n) = G_0^{-1}(i\omega_n) - G_n^{-1}. \quad (6)$$

Equations (4), (5), and (6) constitute the mean-field theory for homogeneous phases. In the limit $d \rightarrow \infty$ Eq. (6) is an exact equation for the lattice problem. We note that for periodic phases, if they exist, one needs to replace the atomic problem by a more complicated many-site problem¹⁷.

These equations are complicated to solve analytically but a simplification occurs for $0 \leq \rho_e \leq 1 - \rho_i$ in the limit $U \rightarrow \infty$. Indeed, when U is large the spectrum of the Hamiltonian consists of two bands separated by a gap of order U for electron fillings that satisfy $0 \leq \rho_e \leq 1 - \rho_i$. In this case the chemical potential lies within the lower band, so that μ is $O(1)$. We note that G_0 is a function of μ , and therefore for any finite μ , $1/[G_0(i\omega_n)U] \rightarrow 0$ as $U \rightarrow \infty$. Then Eq. (4) becomes

$$G_n = (1 - \rho_i)G_0(i\omega_n), \quad (7)$$

and substituting Eq. (7) into Eq. (6) and solving for the self energy, then yields

$$\Sigma_n = -\frac{\rho_i}{G_n}, \quad (8)$$

for the relation between the local self energy and the Green's function. Hence, in the limits $U \rightarrow \infty$ and $d \rightarrow \infty$ the equations for the homogeneous phase reduce to Eqs. (5) and (8).

In the case of the Bethe lattice, $\rho_B(\epsilon) = \sqrt{4 - \epsilon^2}/(2\pi)$, for $-2 < \epsilon < 2$, so that the integral in Eq. (5) can be performed analytically

$$G_n = \frac{i\omega_n + \mu - \Sigma_n}{2} - \frac{1}{2}\sqrt{(i\omega_n + \mu - \Sigma_n)^2 - 4}. \quad (9)$$

Substituting the result from Eq. (8) into Eq. (9) and solving for G_n yields the exact result for the interacting Green's function in the strongly correlated limit

$$G_n = \frac{i\omega_n + \mu}{2} - \frac{1}{2}\sqrt{(i\omega_n + \mu)^2 - 4(1 - \rho_i)}, \quad (10)$$

where the phase of the square root is chosen so that the Green's function has the correct sign to its imaginary part. This form is identical to that of a noninteracting Green's function [Eq. (9) with $\Sigma_n = 0$], with a bandwidth narrowed from 4 to $4\sqrt{1 - \rho_i}$, and containing a spectral weight of $1 - \rho_i$ (since the remaining spectral weight is shifted to infinite energies). This is easiest seen from the interacting density of states, which satisfies¹⁹

$$\rho_B^{int}(\epsilon) = \frac{1}{2\pi}\sqrt{4(1 - \rho_i) - \epsilon^2}. \quad (11)$$

Note that in the infinite-interaction-strength limit, we have an analytic form for the Green's functions, and do not need to iteratively solve transcendental equations as is normally done in the finite- U case.¹⁵ Furthermore, even though the Green's function has the same form as a noninteracting Green's function, the self-energy is nontrivial and does not correspond to a Fermi liquid!

This form for the Green's function fits a rather simple physical picture. The electron avoids sites occupied by an ion when $U \rightarrow \infty$, so the number of available sites is reduced by the fraction $1 - \rho_i$. This means, on average, the number of nearest neighbors is reduced by the same factor, which reduces the bandwidth by $\sqrt{1 - \rho_i}$. The total spectral weight is also reduced from 1 to $1 - \rho_i$, because the upper band (with ρ_i states) is located at infinite energy. What is surprising is that this "hand-waving" argument is exact for the Bethe lattice (we will see below it is a good approximation for the hypercubic lattice, but is not exact).

The interacting density of states is temperature-independent²⁰ in the local approximation, which means that we can examine the ground state at $T = 0$ to see if the system phase separates, or if the homogeneous phase is lowest in energy. The ground state energy for an ion concentration ρ_i and an electron concentration ρ_e is

$$E(\rho_e, \rho_i) = \int_{-\infty}^{\mu} d\epsilon \rho_B^{int}(\epsilon)\epsilon, \quad (12)$$

with μ the chemical potential defined by

$$\rho_e = \int_{-\infty}^{\mu} d\epsilon \rho_B^{int}(\epsilon), \quad (13)$$

and ρ_B^{int} the interacting density of states. Substituting in the exact result from Eq. (11) yields

$$E(\rho_e, \rho_i) = -\frac{4}{3\pi}(1 - \rho_i)^{3/2} \left[1 - \frac{\mu^2}{4(1 - \rho_i)} \right]^{3/2}, \quad (14)$$

and

$$\rho_e = \frac{1 - \rho_i}{\pi} \left[\cos^{-1} \left(\frac{-\mu}{2\sqrt{1 - \rho_i}} \right) + \frac{\mu}{2\sqrt{1 - \rho_i}} \sqrt{1 - \frac{\mu^2}{4(1 - \rho_i)}} \right]. \quad (15)$$

Using Eqs. (14) and (15), we will show that the mixture of the state with no ions and an electron filling $\rho_e/(1 - \rho_i)$ with the state with all ions and no electrons has a lower energy than the homogeneous state, i. e.

$$E(\rho_e, \rho_i) > (1 - \rho_i)E\left(\frac{\rho_e}{1 - \rho_i}, 0\right) + \rho_i E(0, 1). \quad (16)$$

Moreover, from Eq. (16) we will deduce that the mixture corresponding to the right hand side of Eq. (16) has lower energy than any other mixture between homogeneous states. In other words,

$$\alpha E(\rho'_e, \rho'_i) + (1 - \alpha)E(\rho''_e, \rho''_i) > (1 - \rho_i)E\left(\frac{\rho_e}{1 - \rho_i}, 0\right) + \rho_i E(0, 1), \quad (17)$$

where $0 \leq \alpha \leq 1$ and $\rho_e = \alpha\rho'_e + (1 - \alpha)\rho''_e$, $\rho_i = \alpha\rho'_i + (1 - \alpha)\rho''_i$, $0 < \rho'_e < 1 - \rho'_i$, and $0 < \rho''_e < 1 - \rho''_i$. To obtain Eq. (16), we first notice that $E(0, 1) = 0$ and that the chemical potential $\bar{\mu}$ corresponding to an electron filling of $\rho_e/(1 - \rho_i)$ and an ion filling of zero is $\bar{\mu} = \mu/(2\sqrt{1 - \rho_i})$, as can be seen from Eq. (15). Therefore, Eq. (14) yields

$$(1 - \rho_i)E\left(\frac{\rho_e}{1 - \rho_i}, 0\right) + \rho_i E(0, 1) = -\frac{4}{3\pi}(1 - \rho_i) \left[1 - \frac{\mu^2}{4(1 - \rho_i)} \right]^{3/2} = \frac{1}{\sqrt{1 - \rho_i}} E(\rho_e, \rho_i) < E(\rho_e, \rho_i), \quad (18)$$

which proves Eq. (16). The proof of Eq. (17) relies on an application of Eq. (16)

$$\begin{aligned} & \alpha E(\rho'_e, \rho'_i) + (1 - \alpha)E(\rho''_e, \rho''_i) > \\ & \alpha \left[(1 - \rho'_i)E\left(\frac{\rho'_e}{1 - \rho'_i}, 0\right) + \rho'_i E(0, 1) \right] + (1 - \alpha) \left[(1 - \rho''_i)E\left(\frac{\rho''_e}{1 - \rho''_i}, 0\right) + \rho''_i E(0, 1) \right]. \end{aligned} \quad (19)$$

The right hand side of Eq. (19) is equal to

$$(1 - \rho_i) \left[\frac{\alpha(1 - \rho'_i)}{1 - \rho_i} E\left(\frac{\rho'_e}{1 - \rho'_i}, 0\right) + \frac{(1 - \alpha)(1 - \rho''_i)}{1 - \rho_i} E\left(\frac{\rho''_e}{1 - \rho''_i}, 0\right) \right] + \rho_i E(0, 1). \quad (20)$$

On the other hand, $E(\rho_e, 0)$ is a convex function of ρ_e , so the term inside the brackets in Eq. (20) is greater than $E(\rho_e/[1 - \rho_i], 0)$, which yields Eq. (16). We remark that the

convexity of $E(\rho_e, 0)$ is obvious from the fact that the free electron system cannot phase separate. Formally, it can be seen as follows: differentiating Eqs. (14) and (15) with respect to ρ_e gives $E'(\rho_e, 0) = \mu\rho_B(\mu)\partial\mu/\partial\rho_e$ and $1 = \rho_B(\mu)\partial\mu/\partial\rho_e$. Thus $E'(\rho_e, 0) = \mu$ and $E''(\rho_e, 0) = \partial\mu/\partial\rho_e = 1/\rho_B(\mu) > 0$.

Our interest now is to determine the finite-temperature phase diagram of the infinite- U Falicov-Kimball model since we know the system always phase separates at low temperature (although we have not yet ruled out the possibility of charge-density-wave phases being lower in energy than the phase-separated ground state). The first step is to evaluate the conduction electron charge-density-wave susceptibility. It is often stated that the Bethe lattice can only support antiferromagnetic or uniform order—no incommensurate or other “periodic” phases can exist. But this statement has never been proven, and recent work has shown it to be false¹⁷ by a counterexample of a period-three phase stabilized on the infinite-dimensional Bethe lattice at zero temperature. The momentum dependence enters the dressed susceptibility only through the momentum dependence of the bare susceptibility because the vertex function is local in the infinite-dimensional limit. This allows us to simply take the $U \rightarrow \infty$ of the Brandt-Mielsch result¹⁵, which gives

$$1 = \rho_i \sum_{n=-\infty}^{\infty} \frac{G_n^2 + \chi_n^0(X)}{G_n^2 + \rho_i \chi_n^0(X)}, \quad (21)$$

with X being the parameter that determines the modulation of the charge-density-wave over the Bethe lattice and with $\chi_n^0(X)$ the corresponding bare susceptibility. We do not provide the general formula for all possible charge-density waves here. Rather, we present the three simplifying cases for the susceptibility on the Bethe lattice: (i) the local susceptibility, where $\chi_n^0(\text{local}) = -G_n^2$; (ii) the ($X = -1$) “antiferromagnetic” susceptibility, where

$$\chi_n^0(-1) = -\frac{G_n}{i\omega_n + \mu - \Sigma_n}; \quad (22)$$

and (iii) the ($X = 1$) uniform susceptibility, where

$$\chi_n^0(1) = \frac{\partial G_n}{\partial \mu} = -\frac{G_n}{\sqrt{(i\omega_n + \mu - \Sigma_n)^2 - 4}}. \quad (23)$$

The local susceptibility never has a transition, because the numerator of Eq. (21) vanishes. The condition for an “antiferromagnetic” charge density wave becomes

$$1 = \rho_i \sum_{-\infty}^{\infty} \frac{G_n}{i\omega_n + \mu}, \quad (24)$$

after substituting in the infinite- U form for the self-energy, and using the quadratic equation $G_n^2 - (i\omega_n + \mu)G_n + 1 - \rho_i = 0$ that the interacting Green’s function satisfies. Now, substituting the integral form for G_n

$$G_n = (1 - \rho_i) \int_{-\infty}^{\infty} d\epsilon \frac{\rho_B(\epsilon)}{i\omega_n + \mu - \sqrt{1 - \rho_i \epsilon}}, \quad (25)$$

into Eq. (24) and performing the sum over Matsubara frequencies yields the final integral form for T_c

$$1 = -\frac{\rho_i \sqrt{1-\rho_i}}{2T} \int_{-2\sqrt{1-\rho_i}}^{2\sqrt{1-\rho_i}} dz \frac{\rho_B \left(\frac{z}{\sqrt{1-\rho_i}} \right) \tanh \frac{\beta z}{2}}{z \cosh^2 \frac{\beta \mu}{2} (1 - \tanh \frac{\beta \mu}{2} \tanh \frac{\beta z}{2})}, \quad (26)$$

(see Appendix A). But this integrand is positive for all z , so the right hand side is always less than zero, and there is no “antiferromagnetic” T_c . The staggered charge-density-wave order has been found near half-filling $\rho_i = \rho_e = 1/2$ when the lowest-order exchange for finite- U is included,²¹ but can only occur at $T = 0$ and $\rho_i = \rho_e = 1/2$ when $U = \infty$.

The uniform susceptibility case is analyzed as follows: First the uniform susceptibility from Eq. (23) is substituted into Eq. (21), and the square root is eliminated by using the exact form for the interacting Green’s function in Eq. (9). Next, the self energy is replaced by its exact form from Eq. (8), and the quadratic equation for G_n is used to simplify the T_c equation to

$$1 = \rho_i \sum_{n=-\infty}^{\infty} \left[1 + \frac{1 - \rho_i}{(i\omega_n + \mu)G_n - 2(1 - \rho_i)} \right]. \quad (27)$$

Now the interacting form for G_n from Eq. (10) is substituted into Eq. (27) and the results simplified to yield

$$1 = \rho_i \sum_{n=-\infty}^{\infty} \frac{(i\omega_n + \mu)G_n - 2(1 - \rho_i)}{(i\omega_n + \mu)^2 - 4(1 - \rho_i)}. \quad (28)$$

The final step is to substitute in the integral form for G_n from Eq. (25) and perform the summation over Matsubara frequencies (see Appendix A). After making a trigonometric substitution, the transcendental equation for T_c becomes

$$1 = \frac{\rho_i \sqrt{1-\rho_i}}{2\pi T} \int_0^\pi d\theta \cos \theta \tanh \frac{\beta}{2} (2\sqrt{1-\rho_i} \cos \theta - \mu). \quad (29)$$

We do not discuss any of the other periodic cases here, because the numerics involved is cumbersome. But, we expect the Bethe lattice to have similar behavior as the hypercubic lattice, where the transition always went into the uniform charge-density wave, signifying a phase separation transition. Details of the other periodic phases will be reported in a future publication.

The results for the transition temperature for the uniform charge-density wave are presented in Figure 1(a). We choose nine different ion concentrations ranging from 0.1 to 0.9 in steps of 0.1. The electron density then varies from 0 to $1 - \rho_i$ for each case. As can be seen in the figure, the maximal transition temperature is about $0.12t^*$ and it occurs at half-filling of the lower band $\rho_e = (1 - \rho_i)/2$ with $\rho_i \approx 0.65$ (coincidentally, this maximal transition temperature is nearly identical to the maximal T_c to charge-density-wave order at $\rho_e = \rho_i = 1/2$ when evaluated as a function of the interaction strength U). Since $T_c \ll 1$, we expand Eq. (29) for small T by replacing the $\tanh x$ by $\text{sgn} x$ to find

$$T_c \approx \frac{\rho_i \sqrt{1-\rho_i}}{\pi} \sqrt{1 - \frac{\mu^2}{4(1-\rho_i)}}. \quad (30)$$

Since the chemical potential will scale with $\sqrt{1-\rho_i}$ for the same relative electron filling in the lower band $[\rho_e/(1-\rho_i)]$, as shown in eq. (15), this form motivates a scaling plot of

$T_c/(\rho_i\sqrt{1-\rho_i})$ versus $\rho_e/(1-\rho_i)$, which appears in Figure 1(b). As can be seen there, the data nearly collapse on top of each other for T_c which is usually a nonuniversal quantity. In fact, the variation in T_c is less than 10% for all different cases.

The susceptibility analysis shows that the system orders in a uniform charge-density-wave, which indicates that the system will phase separate (or segregate) into two regions, one with a higher concentration of electrons and one with a lower concentration (as we already showed at $T = 0$). Such a phase separation is usually associated with a first-order phase transition, rather than a second-order transition. Hence, it is important to perform a Maxwell construction of the free energy that includes mixtures of two states with different electron and ion concentrations such that $\rho_e = \alpha\rho'_e + (1-\alpha)\rho''_e$, $\rho_i = \alpha\rho'_i + (1-\alpha)\rho''_i$, and that the free energy of the mixture $F(\rho'_e, \rho'_i; \rho''_e, \rho''_i) = \alpha F(\rho'_e, \rho'_i) + (1-\alpha)F(\rho''_e, \rho''_i)$ is lower in energy than the pure-phase free energy $F(\rho_e, \rho_i)$. The second-order phase transition is the spinodal-decomposition temperature, below which the free energy becomes locally unstable in the region of (ρ_e, ρ_i) ; in most cases the global free energy is minimized by the Maxwell construction at a temperature above this spinodal-decomposition temperature. The spinodal-decomposition temperature marks the lowest temperature that the system can be supercooled to before it must undergo a phase transition.

We can calculate the free energy $F(\rho_e, \rho_i)$ for a homogeneous phase with electron filling ρ_e and ion concentration ρ_i in two equivalent ways. The first method is from Brandt and Mielsch¹⁵ which expresses the free energy in terms of a summation over Matsubara frequencies as follows:

$$F(\rho_e, \rho_i) = -T \ln \frac{1 + e^{\beta\mu}}{1 - \rho_i} + \int_{-\infty}^{\infty} d\epsilon \rho(\epsilon) T \sum_{n=-\infty}^{\infty} \ln \left[\frac{i\omega_n + \mu}{(1 - \rho_i)(i\omega_n + \mu - \Sigma_n - \epsilon)} \right] \\ + \mu\rho_e - \left(T \ln \frac{\rho_i}{1 + \rho_i} + T \ln(1 + e^{\beta\mu}) + T \sum_{n=-\infty}^{\infty} \ln \left[\frac{1 - \rho_i}{(i\omega_n + \mu)G_n} \right] \right) \rho_i. \quad (31)$$

Similarly, we can evaluate the free energy in the same fashion as Falicov and Kimball⁵ did

$$F(\rho_e, \rho_i) = T \int_{-\infty}^{\infty} d\epsilon \rho^{int}(\epsilon) \ln \left[\frac{1}{1 + e^{-\beta(\epsilon-\mu)}} \right] + T [\rho_i \ln \rho_i + (1 - \rho_i) \ln(1 - \rho_i)] + \mu\rho_e, \quad (32)$$

where $\rho^{int}(\epsilon) = \sqrt{4(1 - \rho_i) - \epsilon^2}/(2\pi)$ is the interacting density of states for the Bethe lattice. We find that both forms (31) and (32) are numerically equal to each other, but are unable to show this result analytically. Since the interacting density of states is known for the Bethe lattice, we use the computationally simpler form in Eq. (32) in our calculations. For the hypercubic lattice evaluated in Section III, we employ Eq. (31) in the free-energy analysis.

The numerical minimization proceeds in four phases: (i) First a coarse grid is established for ρ'_i and ρ''_i and the free energy is minimized over this grid [the electron fillings are determined by the constraints that the chemical potential is the same in region 1 and region 2 and that $\rho_e = \alpha\rho'_e + (1-\alpha)\rho''_e$, with α already determined from $\rho_i = \alpha\rho'_i + (1-\alpha)\rho''_i$]; (ii) The filling ρ''_i is fixed at its coarse-grid minimal value, and ρ'_i is varied on a finer grid to determine the new minimum; (iii) ρ'_i is fixed at the new minimum and ρ''_i is now varied on a fine grid to yield a new minimal ρ''_i ; (iv) ρ'_i and ρ''_i are varied together on the same fine grid to determine the final minimization of the Maxwell construction. We found that the minimal values of ρ'_i and ρ''_i rarely changed in step (iv) confirming the convergence of this method.

We plot our results in Fig. 2. The first case considered in Fig. 2(a) is the case of relative half filling $\rho_e = (1 - \rho_i)/2$. In this case the chemical potential is always at zero, and the relative electron filling remains unchanged for all ρ_i . The solid line is the first-order transition line and the dotted line is the spinodal-decomposition temperature. The horizontal distance between the solid lines at a fixed temperature is a measure of the order parameter $\rho'_i - \rho''_i$. Notice how the first-order transition temperature is always close to the spinodal-decomposition temperature, but that the difference becomes largest at concentrations close to zero and one. Note further how the two curves meet at the maximum (as they must) where the first-order transition disappears and becomes a second-order transition at a classical critical point. In Fig. 2(b) we plot the phase diagram for the case with $\rho_i = 0.65$ and $\rho_e = (1 - \rho_i)/4$. In this case the chemical potential changes as a function of temperature, and as $T \rightarrow 0$ and the system is phase separating into regions with ion densities close to zero and one, we find that the chemical potential will lie outside of the bandwidth of the interacting density of states as $\rho''_i \rightarrow 1$ because the bandwidth ($4\sqrt{1 - \rho_i}$) becomes narrowed to zero. In that case, the electron density approaches zero exponentially fast, which is why the spinodal-decomposition temperature approaches zero so rapidly in that regime. For this reason, we find that the relative electron filling is not a constant in this phase diagram, as it approaches zero exponentially fast near $\rho''_i = 1$ and it is somewhat larger than quarter filled near $\rho'_i = 0$. The two phase diagrams in Fig. 2(a) and (b) look similar in the low-density regime, however. This may imply that there is an analogous scaling regime for the first-order T_c , but it does not look like there would be a universal curve for the region close to $\rho''_i = 1$. The numerical effort required to perform the free-energy analysis is significant, so a thorough analysis of any possible scaling forms for T_c was not performed.

III. RESULTS FOR THE HYPERCUBIC LATTICE

The formalism for the hypercubic lattice is essentially unchanged from the Bethe lattice. The main differences are that the integrals cannot be performed analytically anymore, which requires results to be worked out numerically, and requires more computational effort. The basic framework in Eqs. (2)—(8) is identical as before, except now the noninteracting density of states is a Gaussian for the hypercubic lattice. The integral for the local Green's function is no longer elementary, and so one needs to solve the problem iteratively as was done previously for the Falicov-Kimball model: (i) first the self energy is set equal to zero; (ii) next the local Green's function is determined from Eq. (5); (iii) then the self energy is determined from Eq. (8); (iv) then steps (ii) and (iii) are repeated until the equations converge. We can compare the results of the interacting Green's function to the form found before for the Bethe lattice, by approximating the interacting density of states in the same fashion as before: we narrow the Gaussian by the factor $\sqrt{1 - \rho_i}$ and have a total weight of $1 - \rho_i$ in the density of states. When we compare the Green's function along the imaginary axis at half filling in Fig. 3(a) we find that that approximation works well at high energies, but begins to fail near zero frequency (we chose $\rho_e = 1/6$, $\rho_i = 2/3$, and $T = 0.1$). The solid line is the exact result and the dotted line is the approximate (band-narrowed) result. The infinite- U Green's function on the hypercubic lattice is more complicated than on the Bethe lattice and the simple form that describes it for the Bethe lattice no longer holds. This is the main reason why the hypercubic lattice is more complicated to deal with than

the Bethe lattice. To see this more fully, we examine the interacting density of states in Fig. 3(b). The interacting density of states is determined by solving the same equations for the Green's function, but this time on the real axis, rather than the imaginary axis. Notice how the band-narrowed form $\sqrt{1-\rho_i} \exp(-\epsilon^2/[1-\rho_i])/\sqrt{\pi}$ (dotted line) is a reasonable approximation to the interacting density of states (solid line) but that it is too narrow, and it overestimates the peak height.

Since we do not know an analytic form for the interacting density of states, we cannot perform the same kind of analysis that we did before at zero temperature to see if the system is phase separated. But we can examine the finite-temperature phase diagrams in the same manner. The susceptibility diverges whenever Eq. (21) is satisfied. The bare susceptibility now takes the form

$$\chi_n^0(X) = -\frac{1}{2\pi} \int_{-\infty}^{\infty} \rho(y) \frac{1}{i\omega_n + \mu - \Sigma_n - y} \int_{-\infty}^{\infty} dz \rho(z) \frac{1}{i\omega_n + \mu - \Sigma_n - yX - z\sqrt{1-X^2}}, \quad (33)$$

where $X = \lim_{d \rightarrow \infty} \sum_{j=1}^d \cos(k_j)$ for the ordering wavevector \mathbf{k} . The bare susceptibility continues to assume a simple form for the same three cases: (i) $X = 0$ the local susceptibility where $\chi_n^0(0) = -G_n^2$; (ii) $X = -1$ the ‘‘antiferromagnetic’’ susceptibility, where $\chi_n^0(-1) = -G_n/(i\omega_n + \mu - \Sigma_n)$; and (iii) $X = 1$ the uniform susceptibility, where

$$\chi_n^0(1) = \frac{\partial G_n}{\partial \mu} = 2[1 - (i\omega_n + \mu - \Sigma_n)G_n]. \quad (34)$$

If we try to approximate the transition temperature by substituting in the approximate form we have for G_n derived by assuming the interacting density of states has the same shape, but is band narrowed, we find that the T_c 's generated are not accurate at all. Hence, the simple band-narrowing approximation works reasonably well for the Green's function, but is poor for the susceptibility.

Instead, we simply solve for the transition temperatures numerically. We find in every case that we examined that the transition temperature is always highest for $X = 1$ and vanishes for all $X \leq 0$. This is shown in Fig. 4 for the cases of $\rho_e = 1/6, 1/12, 1/24, 1/48, 1/96, 1/192, 1/384,$ and $1/768$ and $\rho_i = 2/3$, which ranges from relative half filling to the low-density regime. We plot $T_c(X)$ and see that the system always favors the uniform charge-density wave, signifying that the system wants to phase separate. We calculate the spinodal-decomposition temperature for phase separation by finding the temperature at which the uniform susceptibility diverges as a function of ρ_e and ρ_i . These temperatures are plotted in Fig. 5(a). This plot looks similar to what we found for the Bethe lattice before, so we try the same scaling form in Fig. 5(b), plotting $T_c/(\rho_i\sqrt{1-\rho_i})$ versus $\rho_e/(1-\rho_i)$. Once again we see a data collapse, but the spread in the T_c 's is somewhat larger than that seen in the Bethe lattice.

Finally, we calculate the full phase diagram for the case of relative half filling $\rho_e = (1-\rho_i)/2$ where $\mu = 0$ in Fig. 6. The form of this result is similar to what was seen in the Bethe lattice. The first-order transition temperature and the spinodal-decomposition temperature meet at the peak of the curve where the first-order transition becomes second order. We did not perform a free-energy calculation at other relative fillings here, because the numerical solution was significantly more difficult due to the fact that we needed to use Eq. (31) rather than the computationally simpler Eq. (32).

IV. CONCLUSIONS AND DISCUSSION

We have provided an exact solution to the spinless Falicov-Kimball model in the strongly correlated limit of $U = \infty$. We only considered the less than unit density cases $0 < \rho_e < 1 - \rho_i$, because they all satisfy a similar functional form. On the Bethe lattice we found that the system always phase separated at $T = 0$ to states where the electrons all moved to one part of the lattice, and the ions moved to the other part. The spinodal-decomposition temperature for segregation solved a simple transcendental equation, which we showed collapsed onto a scaling curve. In addition, we solved for the first-order transition temperature for a select number of cases and discovered that the first-order transition usually occurred quite close to the spinodal-decomposition temperature. On the hypercubic lattice, we found similar results, but had to carry the analysis out numerically for all cases considered. We were able to explicitly show that phase separation precluded incommensurate (or commensurate) charge-density-wave order for the hypercubic lattice.

These results show that when the screened Coulomb interaction is large, or in the alloy picture, when the A ions are extremely different from the B ions, then the system will segregate at low temperatures. This proves the segregation principle for the infinite-dimensional limit, and leads us to believe that it holds for all dimensions (since it has also been demonstrated in one dimension). Future problems to be investigated include a study of the case $\rho_e + \rho_i = 1$, as well as finite Coulomb interaction U . In the unit-density case, we expect charge-density-wave order to be more prevalent, perhaps precluding the segregated phase for all U . When the strength of the Coulomb interaction is reduced, we expect the segregated phase to gradually disappear and be taken over by other phase-separated or charge-density-wave ordered phases.

It is possible that the phenomena described here incorporates the relevant physics of the charge-stripe phases in the cuprate materials: that the stripes occurred because of the strong propensity towards phase separation in the strongly correlated limit. The analogy would stem from considering the down spin electrons of the Hubbard model to be frozen in a particular configuration, and then examine how the mobile up spin electrons react to the down spins. The quantum fluctuations of the Hubbard model are replaced by the thermal fluctuations of the Falicov-Kimball model, and it can be viewed as a simplifying approximation to the charge dynamics of the strongly correlated Hubbard model, but not incorporating the spin dynamics. In this case, as postulated by Emery and Kivelson,²² the stripes would form from a balance between the desire for the system to phase separate, and the long-range Coulomb interaction, which would prevent the electrons from completely separating from the ions. There is evidence for alternative points of view, however. White and collaborators²³ have shown that the Hubbard model on a ladder displays charge-stripe order even without the long-range Coulomb interaction. This order arises from the correlation of the spins and the holes and a desire to reduce the frustration induced by the hole motion. In their picture, the stripe ordering arises completely from a model that includes no long-range forces. Nevertheless, it is our belief that the phase separation exhibited here will be an important element of a complete description of the charge-stripe order in the cuprates and nickelates, because it must occur if U becomes large enough.

ACKNOWLEDGMENTS

J.K.F. acknowledges support of this work from the Office of Naval Research Young Investigator Program N000149610828. J.K.F. also acknowledges the hospitality he received at the Institut de Physique Theorique in Lausanne, where this work was initiated.

APPENDIX A: DERIVATION OF THE TRANSCENDENTAL EQUATIONS FOR T_C ON THE BETHE LATTICE

The derivation of Eqs. (26) and (29) involve summations over Matsubara frequencies, which are performed with the help of the identity

$$\tanh \frac{\beta x}{2} = \frac{2}{\beta} \sum_{n=-\infty}^{\infty} \frac{1}{i\omega_n + x}, \quad (\text{A1})$$

for any real number x . Using Eq. (25) and the change of variables $\epsilon \rightarrow \epsilon/\sqrt{1-\rho_i}$ yields

$$\frac{G_n}{i\omega_n + \mu} = \sqrt{1-\rho_i} \int_{-\infty}^{\infty} \frac{d\epsilon}{\epsilon} \rho_B\left(\frac{\epsilon}{\sqrt{1-\rho_i}}\right) \left[\frac{1}{i\omega_n + \mu - \epsilon} - \frac{1}{i\omega_n + \mu} \right]. \quad (\text{A2})$$

Employing Eq. (A1) then shows that

$$\sum_{n=-\infty}^{\infty} \frac{G_n}{i\omega_n + \mu} = \frac{2\sqrt{1-\rho_i}}{\beta} \int_{-\infty}^{\infty} \frac{d\epsilon}{\epsilon} \rho_B\left(\frac{\epsilon}{\sqrt{1-\rho_i}}\right) \left[\tanh \frac{\beta(\mu - \epsilon)}{2} - \tanh \frac{\beta\mu}{2} \right]. \quad (\text{A3})$$

Eq. (26) then follows from the trigonometric identity

$$\tanh \frac{\beta(\mu - \epsilon)}{2} - \tanh \frac{\beta\mu}{2} = \frac{\tanh \frac{\beta\mu}{2}}{\cosh^2 \frac{\beta\mu}{2} (1 - \tanh \frac{\beta\mu}{2} \tanh \frac{\beta\epsilon}{2})}. \quad (\text{A4})$$

The derivation of Eq. (29) is more involved, but proceeds along the same lines. Using the integral representation in Eq. (25) for G_n , performing a decomposition into simple fractions, and then using the identity in Eq. (A1) produces both

$$\begin{aligned} \sum_{n=-\infty}^{\infty} \frac{(i\omega_n + \mu)G_n}{(i\omega_n + \mu)^2 - 4(1-\rho_i)} &= \frac{\beta}{4} \sqrt{1-\rho_i} \tanh \frac{\beta(\mu - 2\sqrt{1-\rho_i})}{2} \int_{-\infty}^{\infty} d\epsilon \frac{\rho_B(\epsilon)}{2-\epsilon} \\ &\quad - \frac{\beta}{4} \sqrt{1-\rho_i} \tanh \frac{\beta(\mu + 2\sqrt{1-\rho_i})}{2} \int_{-\infty}^{\infty} d\epsilon \frac{\rho_B(\epsilon)}{2+\epsilon} \\ &\quad + \frac{\beta}{4} \sqrt{1-\rho_i} \int_{-\infty}^{\infty} d\epsilon \left[\frac{\rho_B(\epsilon)}{2+\epsilon} - \frac{\rho_B(\epsilon)}{2-\epsilon} \right] \tanh \frac{\beta(\mu - \epsilon\sqrt{1-\rho_i})}{2}, \end{aligned} \quad (\text{A5})$$

and

$$\sum_{n=-\infty}^{\infty} \frac{2(1-\rho_i)}{(i\omega_n + \mu)^2 - 4(1-\rho_i)} = \frac{\beta}{4} \sqrt{1-\rho_i} \left[\tanh \frac{\beta(\mu - 2\sqrt{1-\rho_i})}{2} - \tanh \frac{\beta(\mu + 2\sqrt{1-\rho_i})}{2} \right]. \quad (\text{A6})$$

Now we use the fact that the integrals for the noninteracting Green's function are trivial

$$\int_{-\infty}^{\infty} d\epsilon \frac{\rho_B(\epsilon)}{2 - \epsilon} = \int_{-\infty}^{\infty} d\epsilon \frac{\rho_B(\epsilon)}{2 + \epsilon} = 1, \quad (\text{A7})$$

and subtract Eq. (A5) from Eq. (A6) to obtain

$$\sum_{n=-\infty}^{\infty} \frac{(i\omega_n + \mu)G_n - 2(1 - \rho_i)}{(i\omega_n + \mu)^2 - 4(1 - \rho_i)} = \frac{\beta}{4} \sqrt{1 - \rho_i} \int_{-2}^2 d\epsilon \frac{\epsilon}{\pi \sqrt{4 - \epsilon^2}} \tanh \frac{\beta(\epsilon \sqrt{1 - \rho_i} - \mu)}{2}. \quad (\text{A8})$$

Eq. (29) then follows from the change of variables $\epsilon = 2 \cos \theta$.

REFERENCES

- ¹ L. Onsager, Phys Rev. **65**, 117 (1944).
- ² T. D. Lee and C. N. Yang, Phys. Rev. **87**, 410 (1952).
- ³ W. Metzner and D. Vollhardt, Phys. Rev. Lett. **62**, 324 (1989).
- ⁴ A. Georges, G. Kotliar, W. Krauth, and M. J. Rozenberg, Rev. Mod. Phys. **68**, 13 (1996).
- ⁵ L. M. Falicov and J. C. Kimball, Phys. Rev. Lett. **22**, 997 (1969); R. Ramirez, L. M. Falicov, and J. C. Kimball, Phys. Rev. B **2**, 3383 (1970).
- ⁶ Ch. Gruber and N. Macris, Helv. Phys. Acta **69**, 850 (1996).
- ⁷ T. Kennedy and E. H. Lieb, Physica A **138**, 320 (1986).
- ⁸ U. Brandt and R. Schmidt, Z. Phys. B **63**, 45 (1986).
- ⁹ C. Borgs, R. Kotecky, and D. Ueltschi, Commun. Math. Phys. **181**, 409 (1996).
- ¹⁰ N. Datta, R. Fernandez, and J. Fröhlich, J. Stat. Phys. **84**, 455 (1996).
- ¹¹ Ch. Gruber, N. Macris, A. Messager, and D. Ueltschi, J. Stat. Phys. **86**, 57 (1997).
- ¹² J. K. Freericks and L. M. Falicov, Phys. Rev. B **41**, 2163 (1990).
- ¹³ P. Lemberger, J. Phys. A **25**, 715 (1992).
- ¹⁴ J. K. Freericks, Ch. Gruber, and N. Macris, Phys. Rev. B **53**, 16189 (1996).
- ¹⁵ U. Brandt and C. Mielsch, Z. Phys. B **75**, 365 (1989); **79**, 295 (1990); **82**, 37 (1991).
- ¹⁶ J. K. Freericks, Phys. Rev. B **47**, 9263 (1993).
- ¹⁷ Ch. Gruber, N. Macris, Ph. Roger, and J. K. Freericks (unpublished Diplome, École Polytechnique Fédérale de Lausanne, 1998).
- ¹⁸ J. K. Freericks, Ch. Gruber, and N. Macris, Phys Rev. B **53**, 16189 (1996).
- ¹⁹ P. G. J. van Dongen and C. Leinung, Ann. Physik (Leipzig) **6**, 45 (1997).
- ²⁰ P. G. J. van Dongen and D. Vollhardt, Phys. Rev. Lett. **65**, 1663 (1990); P. G. J. van Dongen, Phys. Rev. B **45**, 2267 (1992); M. H. Hettler, A. N. Tahvildar-Zadeh, M. Jarrell, T. Pruschke, and H. R. Krishnamurthy, Phys. Rev. B **58**, R7475 (1998).
- ²¹ B. M. Letfulov, Eur. Phys. J. B **4**, 447 (1998).
- ²² O. Zahar, S. A. Kivelson, and V. J. Emery, Phys. Rev. B **57**, 1422 (1998).
- ²³ S. R. White and D. J. Scalapino, Phys. Rev. Lett. **80**, 1272 (1998); *ibid.* **81**, 3227 (1998).

FIGURES

FIG. 1. Second-order transition temperature on the Bethe lattice (corresponding to spinodal decomposition). (a) Transition temperature plotted as a function of electron filling. (b) Transition temperature plotted on a scaling curve as a function of relative electron filling.

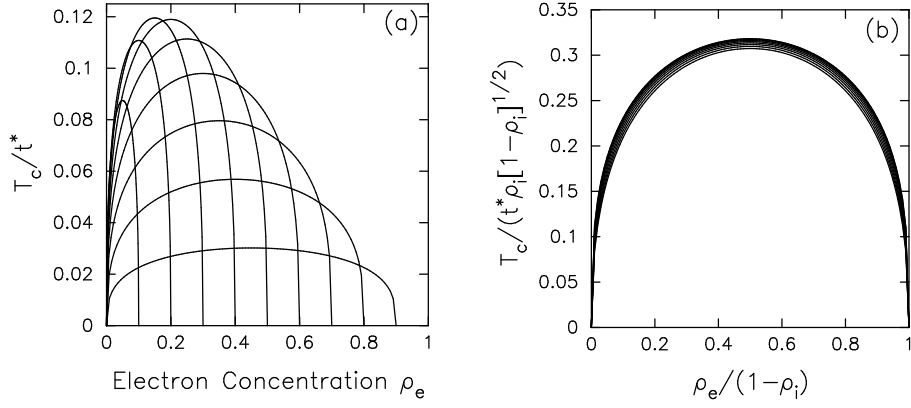
FIG. 2. Transition temperature to phase separation on the Bethe lattice. (a) The case of relative half-filling ($\rho_e = [1 - \rho_i]/2$). The solid line is the first-order transition temperature and the dotted line is the spinodal decomposition temperature. Notice how these two curves meet at the maximum where the first-order transition becomes second order. (b) The case near relative quarter filling (as described in the text). Notice how the shape of the curve differs from (a) near $\rho_i = 1$. This is because the electron filling becomes exponentially small once the chemical potential lies outside of the interacting bandwidth.

FIG. 3. Comparison of the band-narrowed approximation with the exact result on the hypercubic lattice. (a) The Green's function at relative half filling on the imaginary axis. The solid line is the exact result and the dotted line is the approximation. The parameters are $\rho_e = 1/6$, $\rho_i = 2/3$, and $T = 0.1$. (b) The interacting density of states (which is temperature-independent) for the exact (solid line) and approximate (dotted line) cases with $\rho_e = 1/6$ and $\rho_i = 2/3$

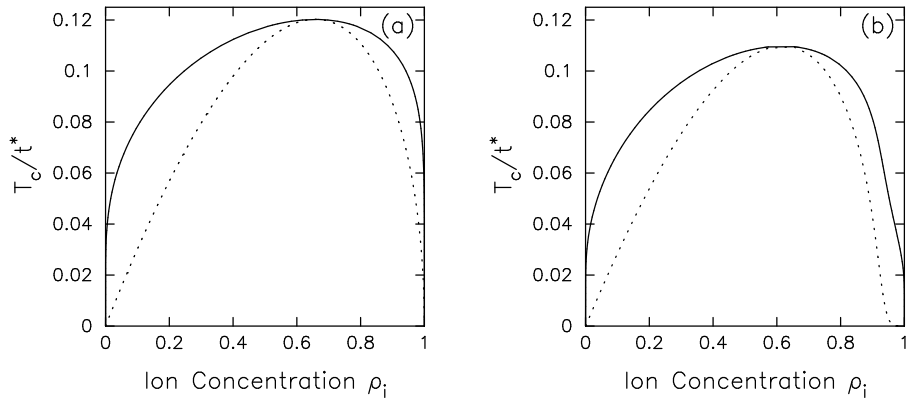
FIG. 4. Plot of the transition temperature versus the ordering wave vector $X(k)$ for the case $\rho_i = 2/3$ and values of ρ_e ranging from relative half filling ($\rho_e = 1/6$) top curve, to the low-density regime ($\rho_e = 1/784$) bottom curve, with the density reduced by a factor of 2 for each case.

FIG. 5. Second-order transition temperature on the hypercubic lattice (corresponding to spinodal decomposition). (a) Transition temperature plotted as a function of electron filling. (b) Transition temperature plotted on a scaling curve as a function of relative electron filling.

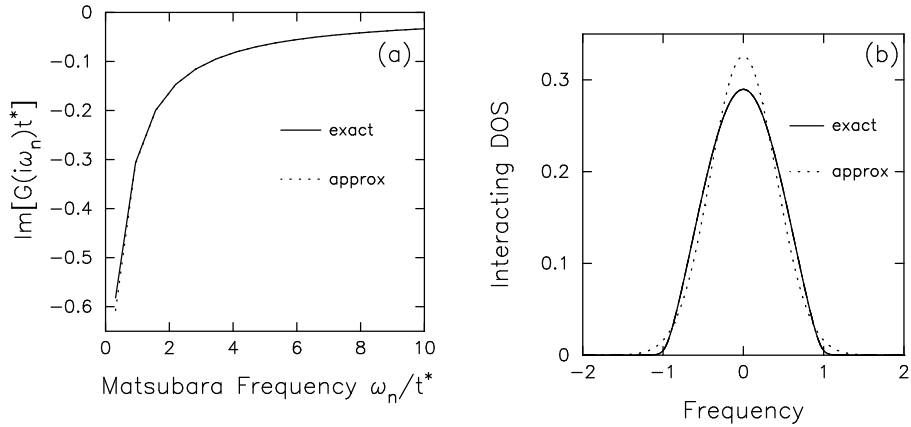
FIG. 6. Transition temperature to phase separation on the hypercubic lattice for the case of relative half-filling ($\rho_e = [1 - \rho_i]/2$). The solid line is the first-order transition temperature and the dotted line is the spinodal decomposition temperature. Notice how these two curves meet at the maximum where the first-order transition becomes second order.



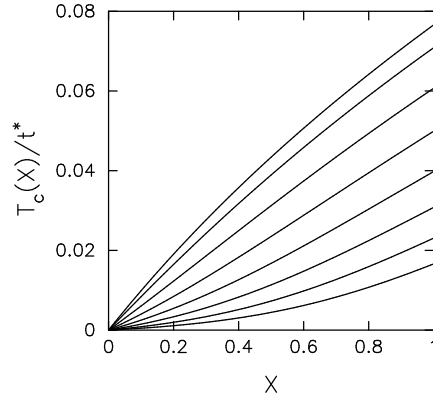
Freericks, et al., Phys. Rev. B, Fig. 1 Freericks, et al., Phys. Rev. B, Fig. 1



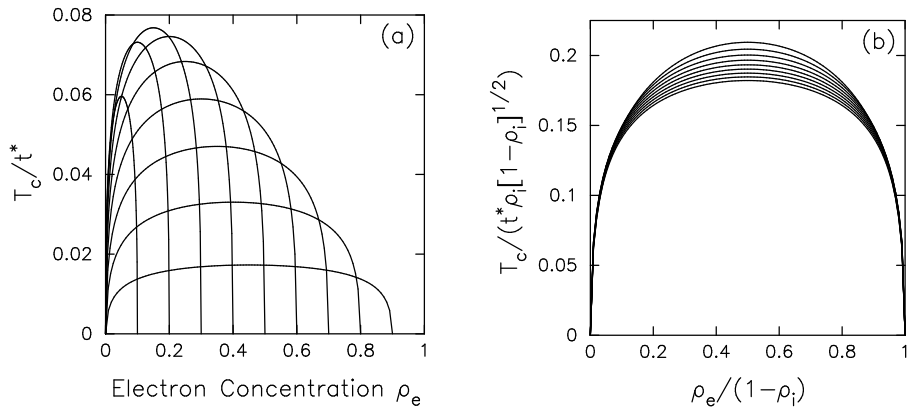
Freericks, et al., Phys. Rev. B, Fig. 2 Freericks, et al., Phys. Rev. B, Fig. 2



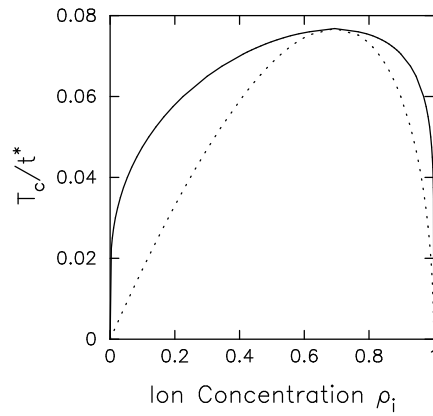
Freericks, et al., Phys. Rev. B, Fig. 3 Freericks, et al., Phys. Rev. B, Fig. 3



Freericks, et al, Phys. Rev. B, Fig.4



Freericks, et al., Phys. Rev. B, Fig. 5 Freericks, et al., Phys. Rev. B, Fig. 5



Freericks, et al., Phys. Rev. B, Fig. 6